Modal degeneracy in thermally loaded optical resonators

Amber L. Bullington,* Brian T. Lantz, Martin M. Fejer, and Robert L. Byer

E. L. Ginzton Laboratory, Stanford University, Stanford, California, USA

**Corresponding author: abull@stanford.edu*

We characterize thermally-induced effects in an optical resonator illuminated with high-power laser radiation. From thermoelastic deformation of a mirror's surface, we observe degeneracy of higher-order spatial modes with the fundamental mode that leads to power transmission limits and thermally-induced power fluctuations using a ring resonator with calibrated absorption loss. A model used to predict the thermal distortion shows reasonable agreement with experiments. Predictions for two future upgrades to the Laser Interferometer Gravitational-wave Observatory (LIGO) show that coating absorption should be less than 3.8 ppm and 0.44 ppm for Enhanced and Advanced LIGO Fabry-Perot cavities, respectively, to avoid the first higher-order modal degeneracy.

OCIS codes: 140.0140, 140.4780, 140.6810, 230.5750, 260.5740.

1. Introduction

The sensitivity for gravitational-wave detection using LIGO, the Laser Interferometer Gravitational-wave Observatory, is limited by shot noise above 250 Hz [1], making increased laser power desirable for detecting gravitational-wave signals above this frequency. The planned upgrade to LIGO, known as Advanced LIGO, calls for a twenty-fold increase in incident laser power to 200 W compared to LIGO's current 10-W laser [1]. An interim upgrade to the detector, Enhanced LIGO, utilizes an increase in laser power to 35 W [2]. Thermally-induced distortion of interferometer optics from thermal lensing and thermoelastic deformation can limit improvements to detector sensitivity [3]. While thermal lensing can significantly impact the beam coupled into and out of a stable optical resonator, thermoelastic deformation alters the eigenmodes of a cavity. In this paper, we focus on thermoelastic deformation and its consequences for LIGO.

Thermoelastic deformation of a mirror's surface from the high circulating power inside an optical resonator may limit the performance of Enhanced and Advanced LIGO. Resonators

experiencing the highest thermoelastic deformation include Fabry-Perot cavities in the arms of the Michelson interferometer that comprises LIGO and the ring resonators that provide input-beam spatial and spectral filtering. Absorption in highly reflecting dielectric coatings dominates the thermoelastic deformation in these cavities. While coating absorption of 1 ppm or less is achievable with current coating technology, thermal effects remain a concern for future LIGO interferometers. For example, the circulating power in the Advanced LIGO arm cavities is proposed to reach 800 kW.

An optical ring cavity, known as a modecleaner, has been designed with calibrated absorption loss to study the effects of thermal loading in an optical resonator with available laser power. LIGO modecleaners spatially and temporally filter the input beam to the interferometer. Figure 1(a) shows a schematic of a table-top modecleaner. It consists of mirrors attached to a fused silica spacer with drilled openings for the circulating beam to traverse free space. The curved mirror is attached to a piezo-electric transducer (PZT) for adjusting the cavity length. All mirrors have low absorption-loss dielectric coatings. The three-bounce geometry is advantageous for separating the reflected beam from the incident beam to avoid back-reflections and eliminates the need for polarizing optics for Pound-Drever-Hall locking of the cavity to resonance [4].

A calibrated absorption loss is achieved by using an infrared-absorbing glass for the substrate of the curved mirror, M_3. Light at the 1064-nm operating wavelength that leaks through the dielectric coating of M_3 is absorbed in a thin layer of the substrate beneath the coating. A low-loss coating on a highly absorbing substrate gives a more effective calibrated absorption loss than a weakly absorbing coating because of better uniformity and linear absorption [5].

Two modecleaners with different absorption loss are illuminated with a 30-W laser. All mirrors for both modecleaners have the same low-loss dielectric coatings. The curved mirror, M_3, of one modecleaner is made of an IR-absorbing glass while the other modecleaner's M_3 has a low-loss substrate. The modecleaner with calibrated absorption loss is referred to as the absorbing modecleaner, while the other is known as the low-loss modecleaner. We start by presenting a model for evaluating the thermoelastic deformation from laser heating, followed by a discussion of experimental results. Finally, predictions for the thermal performance of future LIGO resonators are discussed.

2. Thermally Induced Distortion

In this section we present a model for thermoelastic deformation due to power absorbed in a mirror from an incident Gaussian laser beam. Changes in a resonator's characteristics, namely eigenmode waist size and cavity g-factor product, $g_1 g_2$, are determined. We then discuss how higher-order mode resonance frequencies shift as a function of absorbed power

and determine accidental degeneracies with the fundamental mode.

2.A. Model for Thermoelastic Deformation

Absorption in dielectric coatings and the subsequent thermoelastic deformation of optical surfaces may be a significant cause of reduced transmission in an optical resonator. By assuming that the deformation in the vicinity of the beam waist at a mirror's surface is spherical, Winkler, et. al. [6] approximate the thermoelastic deformation as a change in the depth of curvature or sagitta across the incident Gaussian beam diameter. The relation between undistorted (cold) sagitta, s_{cold}, and radius of curvature, R_{cold}, is given by

$$R_{cold} = \frac{w_{cold}^2}{2s_{cold}}. \tag{1}$$

where w_{cold} is the unperturbed beam radius incident on the mirror. The change in sagitta (δs) of a mirror is related to absorbed power (P_{abs}) in its coating via

$$\delta s = \frac{\alpha}{4\pi\kappa} P_{abs}. \tag{2}$$

α and κ are the thermal expansion coefficient and the thermal conductivity of the optical substrate, respectively [6]. The intracavity circulating power on resonance, P_{circ}, is related to the input power, P_{in} by

$$\frac{P_{circ}}{P_{in}} = \frac{T_1}{(1 - \sqrt{R_1 R_2 R_3 (1 - l_c)})^2} \tag{3}$$

where T_1 and l_c are the input-mirror power transmissivity and cavity losses, respectively [7]. R_1, R_2, and R_3 are the reflectivities of mirrors M_1, M_2, and M_3 in Figure 1(a). To find a simplified expression relating maximum circulating power and finesse, we assume that $R_i = 1 - T_i$ and define $l_{RT} = T_1 + T_2 + T_3 + l_c$ as the power loss in one round trip of the cavity. The denominator of Eqn. (3) can be written as

$$(1 - \sqrt{(1 - T_1)(1 - T_2)(1 - T_3)(1 - l_c)})^2 \approx (1 - \sqrt{1 - l_{RT}})^2 \approx (\tfrac{1}{2} l_{RT})^2. \tag{4}$$

The expression for the circulating power simplifies to

$$\frac{P_{circ}}{P_{in}} \approx \frac{4T_1}{l_{RT}^2}. \tag{5}$$

Power absorbed by the mirror is given by

$$P_{abs} = a_c P_{circ}, \tag{6}$$

where a_c is the mirror absorption. From Siegman [7], cavity finesse can be written approximately as $2\pi/l_{RT}$, giving a simple relation between circulating power and finesse, F, as

$$\frac{P_{circ}}{P_{in}} \approx \frac{2T_1}{\pi l_{RT}} F. \tag{7}$$

For modeling purposes, the ring-resonator geometry of a modecleaner has a two-mirror equivalent cavity that consists of a flat mirror spaced half the modecleaner's perimeter, $L_m = p_m/2$, as shown in Figure 1(b). From Winkler et. al. [6], the change in beam radius at M_1 from distortion of M_3 is given by

$$\frac{\delta w_{1,M_3}}{w_1} = -\frac{\pi}{2\lambda}\frac{\delta s_3}{[g_1 g_2(1-g_1 g_2)]^{1/2}} \tag{8}$$

where λ is the wavelength of light, w_1 the beam radius at M_1, δs_3 the sagittal change at M_3, and g_1 and g_2 are the g-factors ($g = 1 - L/R$) of the two-mirror equivalent resonator. A two-mirror, modecleaner-equivalent cavity has $g_1 = 1$ and $g_2 = 1 - L_m/(R_{cold,M_3})$, where R_{cold,M_3} is the undistorted radius of curvature of M_3.

For the absorbing modecleaner, the small thermoelastic deformation of M_1 and M_2 can be neglected compared to the deformation of mirror M_3. Thus, any contribution to the distortion of the eigenmode waist radius from these optics is neglected. From Eqn. 1 the thermally altered, 'hot' radius of curvature of a mirror is $R_{hot} = w_{hot}^2/(2s_{hot})$, where the hot beam radius and sagitta are given by

$$w_{hot} = w_{cold} - \delta w \tag{9}$$

and

$$s_{hot} = s_{cold} - \delta s. \tag{10}$$

Note that the minus sign in Eqn. 8 results in an increase in beam radius with a corresponding decrease in sagitta. Thus, mirror radius of curvature increases with absorbed power.

The thermally-induced change in curvature has important consequences when considering the modal frequency spacing of a thermally loaded cavity. The impact of the thermally-induced change in modecleaner length on modal frequency spacing is small compared to the change in radius of curvature of the cavity's mirrors [8], implying that any change in cavity g-factors may be approximated as a change in radius of curvature alone. For example, the hot g-factor product, $g_1 g_{2,hot}$, of the equivalent two-mirror absorbing modecleaner is written as

$$g_1 g_{2,hot} = 1 - \frac{L_m}{R_{hot,M_3}}. \tag{11}$$

The modal frequency spacing and higher-order modal degeneracies for a thermally loaded cavity is calculated from this hot g-factor product.

2.B. Higher-Order Mode Spacing

Thermoelastic deformation of resonator-mirror curvature and the resulting change in $g_1 g_2$ alter the resonance frequency of all modes supported by a cavity. Eigenmode resonance

frequencies in an optical resonator, $\omega_{\sigma q}$, normalized by the axial mode spacing, $\Delta\omega_{ax}$, give $\overline{\omega}_{\sigma q} = \omega_{\sigma q}/\Delta\omega_{ax}$ and are related to $g_1 g_2$ by

$$\overline{\omega}_{\sigma q} = q + \frac{\sigma + 1}{\pi} \cos^{-1}[(g_1 g_2)^{1/2}] \tag{12}$$

where $\overline{\omega}_{\sigma q}$ is the normalized frequency of the q^{th} axial mode, σ is the mode-index sum, and $g_1 g_2$ is the g-factor product [7]. For a Hermite-Gaussian mode represented by TEM_{mn}, $\sigma = m + n$, where m and n are the number of nodes in the horizontal and vertical directions, respectively. Similarly, $\sigma = 2p + l$ for a Laguerre-Gaussian mode represented by LG_{pl}, where the number of radial and azimuthal nodes are given by p and l, respectively.

The three-bounce geometry of a modecleaner results in an additional π phase shift for higher-order modes with certain symmetry. This additional π phase shift resets their resonance frequency by half the axial mode spacing. For TEM_{mn} modes with m odd and LG_{pl} modes with l even and $l > 0$, the modal resonance is given by

$$\overline{\omega}_{\sigma^* q} = q + \frac{\sigma^* + 1}{\pi} \cos^{-1}[(g_1 g_2)^{1/2}] + \frac{1}{2} \tag{13}$$

where σ^* indicates the given mode-index sum requires this additional frequency shift. In any resonator with an odd number of reflections, this additional π phase shift occurs for odd TEM_{mn} and even LG_{pl} eigenmodes regardless of polarization. A resonator with even-numbered reflections, such as a two-bounce or four-bounce cavity, does not have any eigenmodes with shifted resonance frequencies.

In general, a higher-order mode can become degenerate with the fundamental mode when

$$\overline{\omega}_{\sigma q'} - \overline{\omega}_{0q} = \frac{\sigma}{\pi} \cos^{-1}[(g_1 g_{2,hot})^{1/2}] + (q' - q) = k \tag{14}$$

or

$$\overline{\omega}_{\sigma^* q'} - \overline{\omega}_{0q} = \frac{\sigma^*}{\pi} \cos^{-1}[(g_1 g_{2,hot})^{1/2}] + \frac{1}{2} + (q' - q) = j \tag{15}$$

where k and j are integers. The change in modal resonance frequency with respect to $g_1 g_{2,hot}$ is dependent on the mode-index sum, σ or σ^*. Figure 2 shows a plot of normalized resonance frequency versus $g_1 g_2$ for the TEM_{00} and $TEM_{11,0}$ modes of a modecleaner, showing how the resonance frequency of $TEM_{11,0}$ changes considerably compared to the fundamental-mode resonance. (The choice of $TEM_{11,0}$ will become apparent in section 3.) The cold-cavity g-factor product, $g_1 g_2$, of a modecleaner is 0.79, as marked by a vertical line on the plot. Thermally loading a modecleaner increases the cavity's g-factor product, resulting in a potential overlap in resonance of a higher-order mode with the fundamental mode. Figure 2 shows the $TEM_{11,0}$ mode overlapping with the TEM_{00} mode for a hot g-factor product, $g_1 g_{2,hot}$, of 0.8274. This modal degeneracy significantly impacts resonator transmission with important consequences for gravitational-wave detection as will be discussed in subsequent sections.

3. Thermal Loading Experiment

Figure 3 shows a schematic of the experimental layout for testing the thermal response of a modecleaner. A 30-W Nd:YAG Master Oscillator Power Amplifier (MOPA) laser beam is filtered with a finesse-of-50 'filter modecleaner' to produce a spatially filtered fundamental mode with no discernable higher-order modal content. The filtered beam is subsequently mode-matched into the modecleaner to be tested under thermal load, known as the 'cavity under test.' The filter modecleaner and cavity under test are locked to resonance using the Pound-Drever-Hall technique. The transmitted beam is then analyzed for higher-order modal content with a 'mode analyzer.' The mode analyzer's length is linearly scanned using the PZT attached to mirror M_3 to measure the fundamental-mode power coupled into the cavity. Higher-order mode content of this beam is also measured with the same cavity scan. The transmission of the cavity under test is also analyzed for power variation through a data acquisition system. The filter modecleaner, cavity under test, and mode analyzer are identical in geometry with a perimeter, p_m, of 42 cm and M_3 radius of curvature of 1 m. Table 1 lists relevant parameters of each cavity.

A modecleaner can be tested under different conditions depending on the polarization of the incident light. S-polarized light experiences an additional π phase shift inside a modecleaner relative to p-polarized light, causing the resonances of the two polarizations to not overlap in frequency. This allows a modecleaner to be locked to one polarization with excellent rejection of the orthogonal polarization [9]. Each polarization state also has a different reflectivity for M_1 and M_2 and hence a different finesse, allowing a modecleaner to be thermally loaded with differing levels of input power depending on the intracavity enhancement of a given input polarization, as listed in Table 1.

3.A. Measurements of Thermal Loading in the Absorbing Modecleaner

3.A.1. P-Polarized Cavity

The absorbing modecleaner is illuminated with p-polarized light and locked on resonance with the Pound-Drever-Hall technique. Incident power is increased in steps and the cavity relocked at each power increment. Figure 4 shows a plot of fundamental-mode content as a function of power absorbed by M_3 for incident power up to 6 W. As shown in Table 1, the input power is enhanced by a factor of 105 inside the cavity. The absorbing modecleaner's transmitted beam is scanned in the mode-analyzer cavity and coupled fundamental-mode content is measured. Absorbed power, P_{abs}, is calculated from measured transmitted power, P_{trans}, from the absorbing modecleaner and its coating transmissions via

$$P_{abs} = \frac{T_3}{T_2} P_{trans}, \tag{16}$$

where T_2 and T_3 are the power transmissions of mirrors M_2 and M_3, respectively. For the absorbing modecleaner, $T_3/T_2 = 0.01$.

As shown in Figure 4, the fundamental-mode content decreases rapidly beyond 40 mW of absorbed power but also dips at specific absorbed powers as the thermal load is increased. The first dip in fundamental-mode transmission occurs at 9 mW of absorbed power, resulting in a 1-% drop in fundamental-mode content. A 7-% dip occurs at 35 mW of absorption. Power coupled to the LG_{23} and $TEM_{11,0}$ modes at 9 mW and 35 mW, respectively, dominates these degradations of the transmitted beam. Thermal distortion increases the radius of curvature of mirror M_3, causing the resonance frequencies of higher-order modes to shift such that they become degenerate with the fundamental mode. The curvature mismatch between the distorted mirror and cavity field allows coupling of power into these higher-order modes. At absorption levels where specific higher-order mode coupling is not observed, a maximum of 2 % of power is coupled into the TEM_{20} and TEM_{02} modes from the change in cavity eigenmode waist compared to the incident beam radius. Other higher-order modes are also resolved by the mode analyzer at these absorption levels but contain an insignificant amount of power. For example, the LG_{13} and LG_{33} modes are also measured with the mode analyzer at 9 mW of absorption but contain a negligible amount of power. The same results are observed at 35 mW absorbed power with small power coupling to the $TEM_{13,0}$ and TEM_{90} modes in addition to the $TEM_{11,0}$ mode.

Figure 5(a) shows a CCD-camera image of the $TEM_{11,0}$ mode that overlaps with the fundamental mode of the absorbing modecleaner. Figure 5(b) shows the same $TEM_{11,0}$ mode after filtering through the mode analyzer.

As the absorbed power is raised beyond 40 mW, the absorbing modecleaner's transmitted power no longer increases linearly with input power as strong coupling to the LG_{12} mode draws power from the fundamental mode. Figure 5(c) shows the highly distorted transmitted beam at 47 mW of absorption, while Figure 5(d) clearly demonstrates, using the mode analyzer, that the overlapping mode is LG_{12}. Coupling to other higher-order modes is minimal; the measured LG_{22} mode contains 17$\times$ less power than the LG_{12} mode.

Figure 6 shows that the absorbing modecleaner's transmitted power fluctuates as a function of time for 47 mW of absorbed power (6 W incident power). At 47 mW of absorption and beyond, steady, locked transmitted power from the absorbing modecleaner is no longer achieved. A thermally dependent, periodic-power fluctuation causes the transmitted power to vary by as much as 75 % at frequencies ranging from 14 Hz to 30 Hz. The depth of the fluctuation increases with absorption while the frequency decreases until the servo can no longer maintain lock with the large power variation. During one thermal cycle, the transmitted mode morphs from the fundamental mode to LG_{12}, indicating that significant power is coupled into the LG_{12} mode. Since the cavity cannot support higher-order mode resonance

at maximum power, the overall transmission of the cavity must decline. As M_3 of the absorbing modecleaner cools from the decline in thermal load, power may again build up in the fundamental mode, allowing the cycle to repeat. The authors are currently developing a model for this phenomenon. The onset of this thermally-induced variation in transmission represents a thermal limit for a resonant cavity for gravitational-wave detection.

Figure 7 shows the g-factor product, $g_1 g_2$, as a function of absorbed power for the modecleaner. The predicted modal overlaps versus absorbed power with indicated mode-index sums are highlighted on the graph. Higher-order mode overlap with the fundamental mode is used to estimate the thermal distortion of a cavity's mirrors. When a higher-order mode overlaps in frequency with the fundamental mode, the new hot-cavity g-factor product can be deduced. The particular mode observed experimentally for a given mode-index sum may be governed by numerous factors such as astigmatism, scatter, and optic imperfections. For example using Eq. (15), the q^{th} axial LG_{12} mode with mode-index sum of 4 overlaps with the $(q^{th} - 1)$ axial fundamental mode when a modecleaner's g-factor product is equal to 0.8536. From this new g-factor product, the hot radius of curvature of the absorbing modecleaner's curved mirror is calculated to be 1.43 m, implying a 40 % change in curvature from the undistorted curvature of 1 m. A calculation of the absorbed power from this new radius of curvature gives an absorption of 45 mW, which agrees with the measured 44 - 47 mW range of absorbed power where the LG_{12} mode is observed. The maximum curvature change of 40 % implies the size of the cavity eigenmode waist increases by 7 %. This change in eigenmode size alters the overlap between the cavity eigenmode and input mode by about 1% [10, 11], implying that higher-order modal degeneracy can degrade beam quality significantly prior to any substantial thermally-induced alteration of the resonator eigenmode.

Table 2 summarizes the calculated and measured absorption from the observed overlapping higher-order modes and the calculated, thermally distorted radius of curvature of M_3. Disagreements between calculated and measured absorption may arise from a thermally-dependent resonance-frequency shift. An, et. al. [12] have shown that change in cavity length from thermal expansion of optics causes a shift in the resonance frequency proportional to the intracavity power. Thus, as the cavity's frequency shifts with increasing thermal load, a broader range of absorption allows for overlap between a higher-order and fundamental mode. This thermally-dependent frequency shift gives an estimated 8× broader frequency range of overlap compared to the cold-cavity linewidth when coupling to the LG_{12} mode is observed.

3.A.2. S-Polarized Cavity

When the absorbing modecleaner is incrementally locked at increasing input power levels in high finesse with s-polarized input light, higher-order modal degeneracy is much stronger

and occurs at a lower absorption threshold than in the p-polarized, low-finesse case. From Eq. (7) and Table 1, the intracavity power enhancement for s-polarization is 1200, while for p-polarization it is 105. The increased power enhancement for s-polarization plays a key role in the degenerate modes observed experimentally.

Results from Figure 7 are applicable for degenerate higher-order modes observed in s-polarization. The first observed modal degeneracy couples 4 % of fundamental-mode power to a $TEM_{9,21}$ mode at 4.25 mW of absorbed power. From Figure 7, observing a mode with index sum of 30 is plausible since the absorption threshold for coupling to these modes is predicted to be near 2.5 mW. The modecleaner aperture diameter is 13× larger than the beam diameter, resulting in low diffraction loss for large-order modes. As the thermal load is increased, strong coupling to multiple higher-order modes rapidly degrades the fundamental-mode transmission with fundamental-mode content dropping to as low as 57 % at 12 mW of absorbed power (300 mW of incident power).

Figure 8 shows a closer view of the mode spectrum transmitted by the mode analyzer when scanned with the absorbing modecleaner's transmission at a thermal load of 10 mW (200 mW of incident power). Coupling to multiple higher-order modes is apparent with strong coupling to one mode spaced closely to the fundamental mode. This strongly coupled higher-order mode is LG_{15}. This mode has a predicted overlap absorption of 14 mW as seen from its mode-index sum of 7 in Figure 7. Observing modal degeneracy with LG_{15} at an absorbed power of 10 mW is in reasonable agreement with the predicted absorption of 14 mW. Strong coupling to higher-order modes that overlap with the fundamental mode may be explained by the higher finesse for s- than for p-polarization. Any higher-order mode degenerate with the fundamental mode sees a power enhancement nearly 12× larger for s-polarization versus p-polarization in a modecleaner. The thermally dependent shift in frequency from thermal expansion of cavity optics also plays a role in the overlap of higher-order modes with the fundamental mode [12]. For example, the resonant frequency shift at 12 mW of absorbed power causes the frequency overlap range of higher-order modes with the fundamental mode to increase by a factor of 25 when compared to the cold cavity linewidth.

3.B. Measurements of Thermal Loading in the Low-Loss Modecleaner

Next, measurements of thermal loading for the low-loss modecleaner with BK7-substrate optics is tested in s-polarization with a power enhancement of 1200. This cavity has 3 ppm absorption losses distributed equally among the mirror coatings. Predictions of modal degeneracy as a function of absorbed power are made with a model similar to the one discussed in Section 2 but also includes thermal deformation of mirrors M_1 and M_2. Transmission increases linearly with input power up to 8 W where 20 mW of absorbed power is reached in the cavity. Beyond 20 mW, higher-order modal degeneracy rapidly degrades the beam

quality. Degenerate higher-order modes also occur at absorptions well below the maximum. The first overlap occurs at 5.1 mW of absorbed power with another overlap at 10 mW of absorption. The large number of nodes in the higher-order modes observed at these absorbed powers make their identification difficult. The $TEM_{0,27}$ and $TEM_{17,0}$ modes are degenerate for 7.1 mW and 9.4 mW absorption, respectively. These degeneracies are calculated from Equations (14) and (15) for the low-loss modecleaner and match well with those observed in the experiment. For p-polarized input, the low-loss modecleaner begins to show some higher-order mode coupling at 5.1 mW of absorption, which is limited by maximum available input power. From these results, the higher-order modal degeneracy is not limited to the characteristics of the absorbing modecleaner but applies to all cavities with similar characteristics. The accidental modal degeneracies are predictable for any resonator configuration if the losses are known.

4. Predictions for Future LIGO Resonators

In this section, predictions of higher-order modal degeneracy with the fundamental mode are determined for resonators experiencing high circulating power in future LIGO interferometers. Resonators that undergo significant thermoelastic deformation from coating absorption include the modecleaners and Fabry-Perot light-storage arm cavities for Enhanced and Advanced LIGO. Since a weak gravitational-wave signal is detected via the resonant fundamental mode of LIGO, higher-order modal degeneracy caused by thermal loading impacts future interferometer performance. To predict the occurrence of higher-order modal degeneracy, new, hot-cavity g-factors are calculated for the maximum thermal load in a given cavity. The new g-factor product is utilized in equations (14) and (15) to find the modes degenerate with the fundamental mode. The coating absorption is assumed to be the same for all resonator mirrors.

4.A. Modecleaners for Enhanced and Advanced LIGO

Modecleaners are employed in two locations for filtering the input beam to the interferometer. A table-top modecleaner identical in geometry to the modecleaners used in the thermal loading experiment provides the initial filtering of the high-power laser. A modecleaner with a perimeter of several tens of meters and suspended mirrors (suspended modecleaner) provides additional spatial and temporal filtering to 10 MHz for the beam incident on the interferometer [13]. These modecleaners utilize mirrors with low-loss coatings on fused silica substrates. While the thermal conductivity of fused silica is low, its small thermal expansion coefficient, uniformity and ease of manufacture in large diameter make it a desirable substrate material for LIGO.

Enhanced and Advanced LIGO table-top modecleaners are needed to filter the 35-W and

200-W proposed laser systems, respectively. The table-top modecleaner for Enhanced LIGO has a finesse of 200, while a modecleaner with finesse of 50 is used for Advanced LIGO. Coating absorptions of 6 ppm and 8.5 ppm for the Enhanced and Advanced LIGO table-top modecleaners, respectively, are needed to reach the first modal overlaps that have mode-index sums of 10, 20, 30, etc. For proposed coating absorption loss of 1 ppm, the table-top modecleaners for Enhanced and Advanced LIGO will not experience higher-order modal degeneracy.

However, the suspended modecleaners for Enhanced and Advanced LIGO show sufficient thermal loading for 1 ppm coating absorption to experience some modal degeneracy. Table 3 lists the properties of the suspended modecleaners as well as their modal overlaps. The higher-order modes degenerate with the fundamental mode have large order (mode-index sum of 11 and higher), indicating that a proper choice of aperture may suppress coupling to these modes. The aperture formed by the mirror itself compared with the beam size is insufficient to suppress higher-order modes. Coating absorptions for each Enhanced and Advanced LIGO modecleaner must exceed 4.7 ppm and 4.2 ppm, respectively, to reach a degenerate mode-index sum that is less than 10. Thus, with coating absorptions at 1 ppm or less and proper aperturing, higher-order mode coupling can be avoided in the these cavities at the proposed operating power levels.

4.B. Fabry-Perot Arm Cavities for Enhanced and Advanced LIGO

LIGO has 4-km Fabry-Perot cavities in each arm of its Michelson configuration to increase interaction time with a gravitational wave [1]. These resonators experience the highest circulating power of any cavity employed in LIGO. For 25 W incident on the interferometer for Enhanced LIGO, the arm cavities experience a maximum circulating power of 100 kW [14]. For Advanced LIGO with 125 W incident on the interferometer, the arm cavities will be subjected to 800 kW of circulating power [15]. Table 4 gives a list of arm-cavity parameters.

Figure 9 shows a plot of cavity g-factor product, $g_1 g_2$, versus the coating absorption of a single mirror for the Enhanced LIGO long-radius arm cavities. Mode-index sums for degenerate higher-order modes are marked along the graph. Vertical lines denote the maximum thermal load experienced for a given coating absorption. Diffraction loss also plays a roll in the higher-order modes an arm cavity may support. The maximum mode-index sum supported by a resonator can be approximated by $s_{max} \approx (a/w)^2$, where a and w are the mirror and beam radii, respectively [7]. $s_{max} = 8$ for Enhanced LIGO. From Figure 9, an Enhanced LIGO arm cavity is likely to show modal degeneracy at 800 mW of total coating absorption for an index sum of 7. To avoid this modal overlap, a mirror's coating absorption should be less than 3.8 ppm, demonstrating that low coating absorption is important for minimizing higher-order mode overlap.

Figure 10 shows modal degeneracy occurring in an Advanced LIGO near-spherical arm cavity with modes having index sums less than 8 at 706 mW, 1.76 W, and 3.48 W total coating absorption for mode-index sums of 7, 6 and 5, respectively. The maximum supported mode-index sum, s_{max}, is 8, the same as Enhanced LIGO. Since an Advanced LIGO arm cavity approaches a confocal resonator as it is heated, its g-factor product will decrease until the mirror radii of curvature equals the length of the cavity. This arm cavity is unlikely to become confocal thermally since the mirror radii of curvature must change by nearly a factor of two. Note that the cold Advanced LIGO arm cavity is nearly degenerate with mode-index sum of 8, needing only 14 mW of total coating absorption for degeneracy, making this overlap unavoidable as power is increased. A coating absorption of less than 0.44 ppm must be obtained to avoid the thermally-induced modal overlap at mode-index sum of 7, which may push the absorption-loss limit of available dielectric-coating technology. Furthermore, coating inhomogeneities from dust or other contamination may also induce higher-order modal degeneracy at thresholds lower than those predicted for uniform coating absorption. Coating uniformity will be most critical for the arm cavities of Advanced LIGO.

5. Conclusion

We have shown that thermoelastic deformation from absorbed power in a mirror induces higher-order modal degeneracy with the fundamental mode of a resonator. Using a mode-cleaner with calibrated absorption loss, higher-order mode coupling showed agreement with theoretical values for given absorption. Finesse also governed the strength of the higher-order mode coupling, resulting in greater higher-order mode coupling for higher finesse. A thermally loaded low-loss modecleaner demonstrated that modal degeneracy predictions are possible for any resonator configuration with knowledge of absorption loss and mirror thermal properties.

Based on modeling of the thermally-induced mode overlaps observed experimentally, predictions were made for modal degeneracy in future upgrades to LIGO. Suspended modecleaners for Enhanced and Advanced LIGO may avoid modal degeneracy with proper aperturing for higher-order modes and coating absorption of 1 ppm. While aperture size may suppress some higher order modes in the arm cavities, modal degeneracy is predicted in Enhanced LIGO for coating absorption exceeding 3.8 ppm and in Advanced LIGO for absorption greater than 0.44 ppm.

An interferometer that employs an all-reflective topology may use substrates with better thermal properties (e.g. silicon) than those only available for transmission at the operating wavelength of 1064 nm [16]. For example, the ratio of change in sagitta, δs, of fused silica to silicon is 20, implying that 20$\times$ the power may be absorbed in a silicon substrate than a fused silica one for the same thermoelastic deformation. An all-reflective Sagnac interferometer for

gravitational-wave detection has been demonstrated using silicon optics [17]. Furthermore, silicon may be cooled to cryogenic temperatures where its thermal expansion coefficient approaches zero at 18 K and 120 K [18], helping to avoid any modal degeneracy induced by thermal distortion. Alternative substrates and interferometer topology may be necessary to avoid thermal effects when considering gravitational-wave detectors beyond Advanced LIGO.

Acknowledgements

This work was supported by the National Science Foundation under grant PHY-05-02641. The authors thank members of the LIGO Scientific Collaboration for insightful discussion. A. Bullington also acknowledges support from a National Science Foundation Graduate Research Fellowship. Jerome Degallaix and Eric Gustafson provided valuable suggestions for the development of this work.

References

1. P. Fritschel, "The second generation LIGO interferometers," in *Proceedings of Astrophysical Sources for Ground-Based Gravitational Wave Detectors*, J. M. Centrella, ed. (American Institute of Physics, 2001), pp. 15–23.
2. R. Adhikari, P. Fritschel, and S. Waldman, "Enhanced LIGO," http://www.ligo.caltech.edu/docs/T/T060156-01.pdf.
3. E. D'Ambrosio, LIGO Laboratory, California Institute of Technology, MS 18-34, Pasadena, CA 91125, USA, A. M. Gretarsson, V. Frolov, B. O'Reilly, and P. K. Fritschel are preparing a manuscript to be called "Effects of mode degeneracy in the LIGO Livingston Observatory recycling cavity."
4. R. W. P. Drever, J. L. Hall, F. V. Kowalski, J. Hough, G. M. Ford, A. J. Munley, and H. Ward, "Laser phase and frequency stabilization using an optical resonator," Appl. Phys. B: Photophys. Laser Chem. **31**, 97–105 (1983).
5. C. Janke, "Thermal loading of optical components in interferometric systems," presented at the LIGO Scientific Collaboration Conference, Baton Rouge, LA, USA, March 2001.
6. W. Winkler, K. Danzmann, A. Rudiger, and R. Schilling, "Heating by optical absorption and the performance of interferometric gravitational-wave detectors," Phys. Rev. A **44**, 7022–7036 (1991).
7. A. E. Siegman, *Lasers* (University Science, Mill Valley, Calif., 1986). Errata URL: http://www-ee.stanford.edu/siegman/lasersbookerrata.txt.
8. N. Uehara and K. Ueda, "Accurate measurement of the radius of curvature of a concave mirror and the power dependence in a high-finesse Fabry-Perot interferometer," Appl. Opt. **34**, 5611–5619 (1995).

9. S. Saraf, R. L. Byer, and P. J. King, "High-extinction-ratio resonant cavity polarizer for quantum-optics measurements," Appl. Opt. **46**, 3850–3855 (2007).
10. N. Uehara, E. K. Gustafson, M. M. Fejer, and R. L. Byer, "Modeling of efficient mode matching and thermal-lensing effect on a laser-beam coupling into a mode-cleaner cavity," Proc. SPIE **2989**, 57–98 (1997).
11. H. Kogelnik, "Coupling and Conversion Coefficients for Optical Modes," in *Proceedings of the Symposium on Quasi-Optics*, (Polytechnic Press, Brooklyn, USA, 1964), pp. 333–347.
12. K. An, B. A. Sones, C. Fang-Yen, R. R. Dasari, and M. S. Feld, "Optical bistability induced by mirror absorption: measurement of absorption coefficients at the sub-ppm level," Opt. Lett. **22**, 1433–1435 (1997).
13. D. Tanner, Department of Physics, University of Florida, P.O. Box 118440, Gainesville, FL, 32611 (personal communication, 2007).
14. R. Adhikari, Department of Physics, California Institute of Technology, Physics Department 103-33, Pasadena, CA, 91125 (personal communication, 2007).
15. P. Fritschel, "Advanced LIGO interferometer parameters," http://emvogil-3.mit.edu/ pf/advligo/SYS/ALparameters.htm.
16. K. X. Sun and R. L. Byer, "All-reflective Michelson, Sagnac, and Fabry-Perot interferometers based on grating beam splitters," Opt. Lett. **23**, 567–569 (1998).
17. P. Beyersdorf, "Results from the Stanford 10 m Sagnac interferometer," in *Proceedings of the* 4^{th} *Edoardo Amaldi Conference on Gravitational Waves*, (Classical and Quantum Gravity, 2001), vol. 19, pp. 1585–1589.
18. S. Rowan, J. Hough, and D. R. M. Crooks, "Thermal noise and material issues for gravitational wave detectors," Phys. Lett. A **347**, 25–32 (2005).

List of Figures

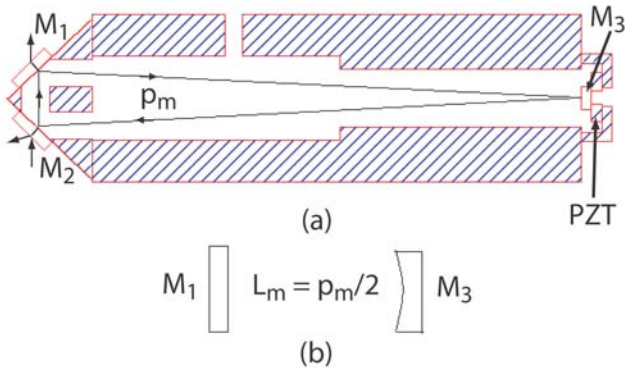

Fig. 1. (Color Online) (a) Schematic of a ring resonator (modecleaner). M_1 and M_2 are 1 inch in diameter, and M_3, attached to a piezoelectric transducer (PZT), is 0.5 inch in diameter with a 1-m radius of curvature. Round-trip perimeter, p_m, is 42 cm. (b) The two-mirror equivalent cavity to a modecleaner for thermal analysis consists of one flat (M_1) and one curved (M_3) mirror spaced $p_m/2$. Bullington-AO90278-fig1.eps

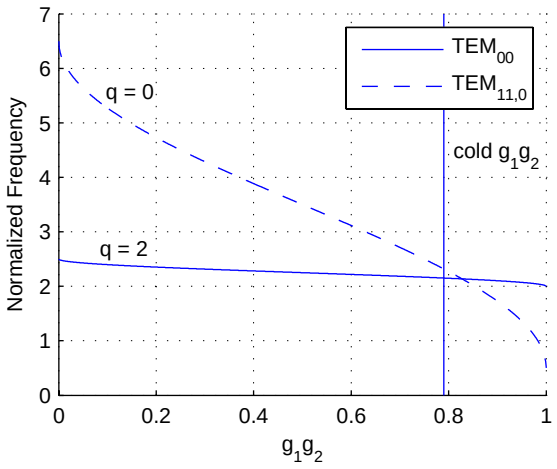

Fig. 2. (Color Online) Normalized modal resonance frequency versus g_1g_2 for the q^{th} axial $TEM_{11,0}$ and $(q^{th}+2)$ TEM_{00} modes of a modecleaner. A vertical line at g = 0.79 indicates a modecleaner's undistorted (cold) g_1g_2. The resonance frequency of $TEM_{11,0}$ changes significantly compared to TEM_{00}, overlapping in resonance with the fundamental mode for $g_1g_2 = 0.8274$. $\sigma = m+n$ for a TEM_{mn} mode. Since σ is odd for $TEM_{11,0}$, this mode's resonance frequency is shifted by half the cavity's axial mode spacing. Bullington-AO90278-fig2.eps

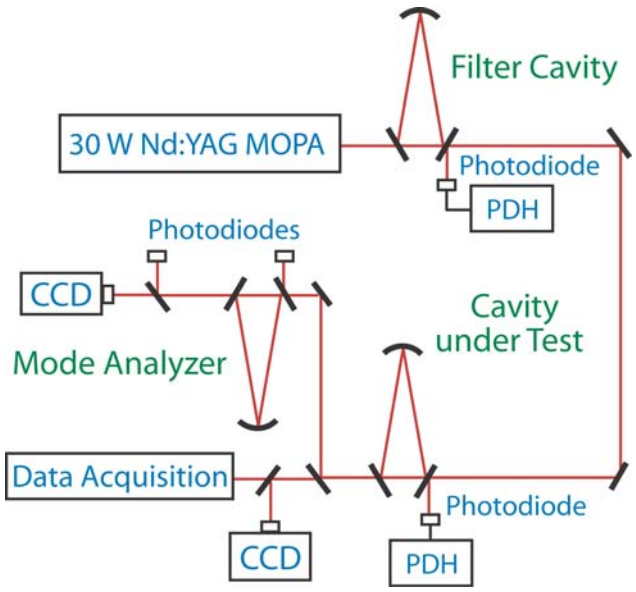

Fig. 3. (Color Online) Experimental layout for testing a ring resonator (modecleaner) under thermal load. A finesse-of-50 modecleaner filters the 30-W Nd:YAG Master Oscillator Power Amplifier (MOPA) system using the Pound-Drever-Hall (PDH) locking technique to provide a spatially filtered, TEM_{00} input beam to illuminate the cavity under test. Output from the cavity under test is transmitted to the mode analyzer and data acquisition system for modal analysis and transmission monitoring. Bullington-AO90278-fig3.eps

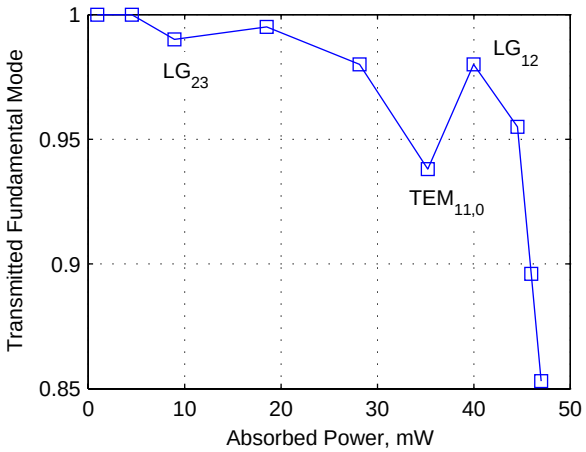

Fig. 4. (Color Online) Transmitted fundamental-mode content of the absorbing modecleaner locked to resonance in p-polarization versus absorbed power as measured with the mode analyzer. Power enhancement in p-polarization is 105 with a maximum input power of 6 W. Beyond 40 mW of absorbed power, the fundamental-mode content rolls off sharply from coupling to the LG_{12} mode. Additional higher-order mode coupling is observed at 9 mW and 35 mW of absorbed power, where power is coupled into the LG_{23} and $TEM_{11,0}$ modes, respectively. Bullington-AO90278-fig4.eps

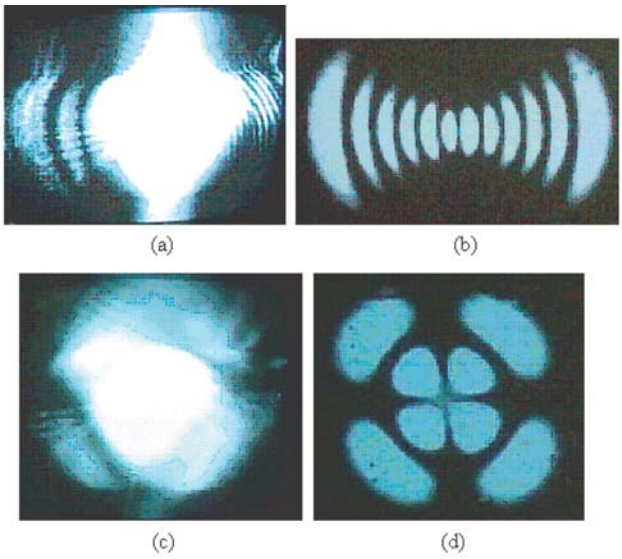

Fig. 5. (Color Online) The CCD image (a) shows that the transmitted beam of the absorbing modecleaner contains both TEM_{00} and $TEM_{11,0}$ modes at 35 mW of absorbed power. The CCD camera is allowed to be slightly saturated to fully resolve the higher-order mode. Image (b) shows the $TEM_{11,0}$ mode when the beam from image (a) is filtered with the mode analyzer. Images (c) and (d) show the absorbing modecleaner's transmitted beam and resultant filtering via the mode-analyzer at 47 mW of absorbed power, clearly showing the higher-order mode is LG_{12}. Bullington-AO90278-fig5.eps

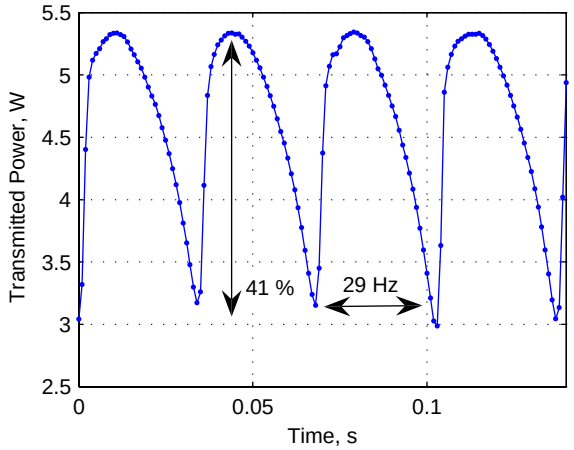

Fig. 6. (Color Online) Periodic fluctuation in transmitted power from the absorbing modecleaner at 6 W incident power. For 47 mW of absorbed power, the transmission of the absorbing modecleaner fluctuates at a frequency of 29 Hz with a fluctuation depth of 41%. Bullington-AO90278-fig6.eps

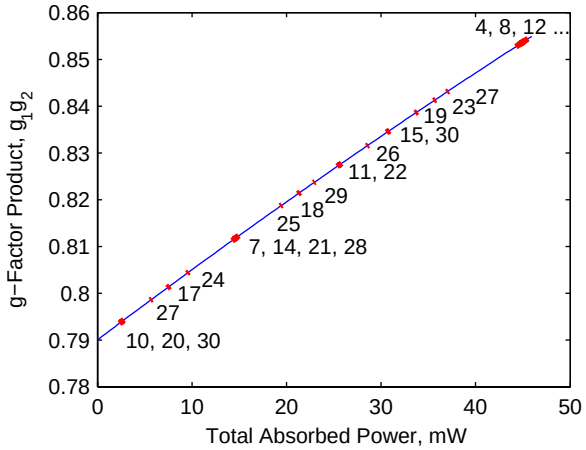

Fig. 7. (Color Online) Absorbing modecleaner's g-factor product, $g_1 g_2$, versus absorbed power. Predicted mode overlaps are highlighted along the curve with the appropriate mode-index sums (defined as $m+n$ for TEM_{mn} modes and $2p+l$ for LG_{pl} modes satisfying Eqns (14) and (15)). This plot applies for both p- and s-polarization, where the intracavity power enhancement is 105 and 1200, respectively. The range of each overlap is estimated from the change in g-factor product needed for a higher-order mode to overlap within the modecleaner's undistorted Full Width at Half Maximum (FWHM) linewidth. Bullington-AO90278-fig7.eps

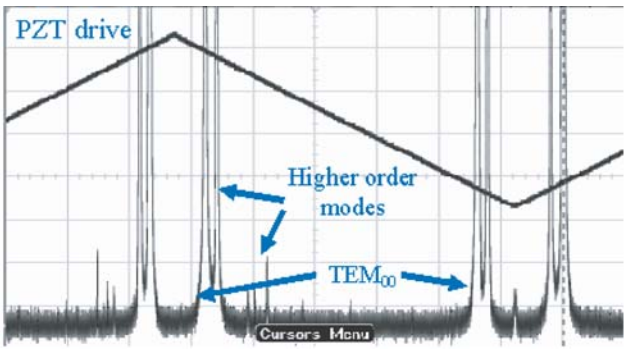

Fig. 8. (Color Online) A close-up of an oscilloscope trace of the transmission of the mode analyzer cavity for the absorbing modecleaner with 10 mW absorption (200 mW input power) in s-polarization. The triangle wave shows the PZT drive signal for the mode analyzer. Coupling to multiple higher-order modes is visible with strong coupling to the LG_{15} mode, which is closely spaced to the fundamental mode. Bullington-AO90278-fig8.eps

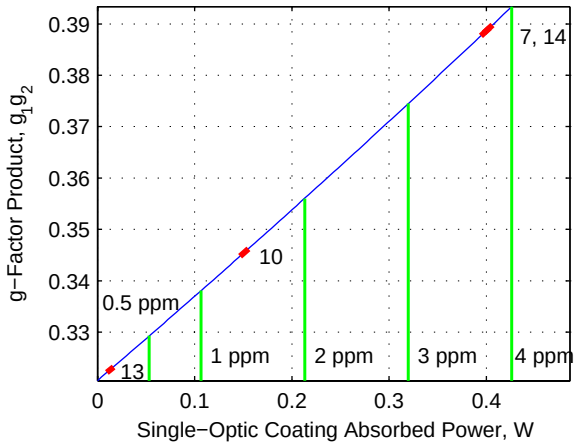

Fig. 9. (Color Online) Enhanced LIGO arm cavity g-factor product, $g_1 g_2$, versus coating absorption of a single optic for 100 kW of circulating power. Predicted mode-index sums giving higher-order modal degeneracy are highlighted along the curve similar to that shown in Figure 7. Vertical lines mark the maximum absorbed power for a given coating absorption. The greater the absorption, the larger the number of possible degenerate higher-order modes. Bullington-AO90278-fig9.eps

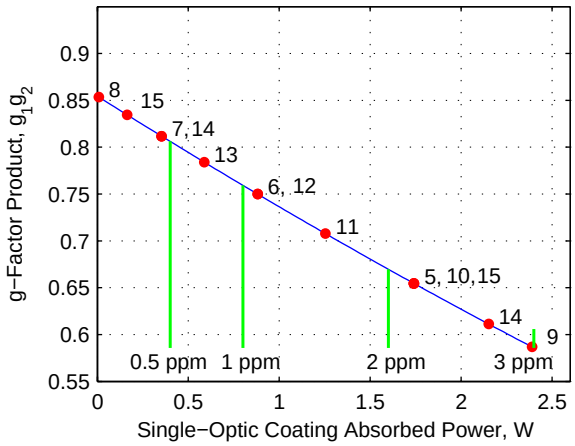

Fig. 10. (Color Online) Advanced LIGO arm cavity g-factor product, $g_1 g_2$, versus coating absorption of a single optic for 800 kW of circulating power. Predicted degenerate mode-index sums are indicated with dots on the graph and vertical lines mark maximum absorbed power for a given coating absorption. Advanced LIGO arm cavities become more susceptible to modal degeneracy at low coating absorption because of high circulating power. Bullington-AO90278-fig10.eps

Table 1. Properties of Modecleaners for Thermal Loading Experiment: Polarization Dependence and Absorption

	Filter Modecleaner	Absorbing Modecleaner	Low-Loss Modecleaner	Mode Analyzer Modecleaner
Absorption	<3.8 ppm	81 ppm	3 ppm	3 ppm
p-pol. Finesse	50	330	330	330
s-pol. Finesse	NA	5500	5500	5500
p-pol. Enhancement[a]	16	105	105	105
s-pol. Enhancement[a]	NA	1200	1200	1200

[a] Enhancement is defined by Eqn 7.

Table 2. Calculated and Measured Absorption in the Absorbing Modecleaner for Three Observed Higher-Order Modes and Calculated Hot Radius of Curvature (ROC)

Observed Mode	LG_{23}	$TEM_{11,0}$	LG_{12}
Calculated Absorption (mW)	14.6	25.6	45
Measured Absorption (mW)	9	35	44-47[a]
M_3 Hot ROC (m)	1.11	1.22	1.43

[a] LG_{12} mode is observed over a range of absorbed powers.

Table 3. Enhanced and Advanced LIGO Suspended Modecleaner Properties and Degenerate Higher-Order Modes for 1 ppm Coating Absorption Loss

Suspended Modecleaner	Enhanced LIGO	Advanced LIGO
Perimeter (m)	24.48	33.33
M_3 Radius of Curvature (m)	17.25	25.95
Finesse	1700	500
Maximum Circulating Power (kW)	15	24
Total Coating Absorption[a] (mW)	23.5	11.5 / 60
Degenerate Mode-Index Sum(s)	11 and 22	22 / 17

[a] Single-optic coating absorption $\times 3$.

Table 4. Enhanced and Advanced LIGO Fabry-Perot Arm Cavity Properties

	Enhanced LIGO[a]	Advanced LIGO[b]
Radius of Curvature (m), M_1	13910	2076
Radius of Curvature (m), M_2	7260	2076
Cavity Length (m)	3995	3995
Optic Radius (cm)	12.5	17
Beam Radius at M_1 (cm)	3.61	5.96
Beam Radius at M_2 (cm)	4.55	5.96
Finesse	220	1257
Maximum Circulating Power (kW)	100	800

[a] Enhanced LIGO arm cavity properties are from the LIGO site in Hanford, WA.

[b] Advanced LIGO data are based on the latest design information [15].